10-24-2017

A Vertical Axis Rotor for Wave Energy Conversion

Yingchen Yang
The University of Texas Rio Grande Valley, yingchen.yang@utrgv.edu

Joab Soto
The University of Texas Rio Grande Valley

Francisco Salazar
The University of Texas Rio Grande Valley

Recommended Citation

Yang, Y, Soto, J, & Salazar, F. "A Vertical Axis Rotor for Wave Energy Conversion." Proceedings of the ASME 2017 Fluids Engineering Division Summer Meeting. Volume 1B, Symposia: Fluid Measurement and Instrumentation; Fluid Dynamics of Wind Energy; Renewable and Sustainable Energy Conversion; Energy and Process Engineering; Microfluidics and Nanofluidics; Development and Applications in Computational Fluid Dynamics; DNS/LES and Hybrid RANS/LES Methods. Waikoloa, Hawaii, USA. July 30–August 3, 2017. V01BT08A007. ASME. https://doi.org/10.1115/FEDSM2017-69458

Proceedings of the ASME 2017 Fluids Engineering Division Summer Meeting
FEDSM2017
July 30-August 3, 2017, Waikoloa, Hawaii, USA

FEDSM2017-69458

A VERTICAL AXIS ROTOR FOR WAVE ENERGY CONVERSION

Yingchen Yang*
University of Texas Rio Grande Valley
Brownsville·Edinburg, Texas, USA

Joab Soto
University of Texas Rio Grande Valley
Brownsville·Edinburg, Texas, USA

Francisco Salazar
University of Texas Rio Grande Valley
Brownsville·Edinburg, Texas, USA

ABSTRACT

The present work augments vertical-axis unidirectional wave energy converter (WEC) designs with a new approach. The enabling technique is the hydrodynamic design of a special rotor, which consists of a series of uniquely shaped blades in a certain formation. Specifically, individual blades are realized by revolving a two-dimensional symmetric hydrofoil about its chord line. Then the blades are arranged around a vertical shaft in a desired formation to form the rotor. When driven by an approaching flow through interaction, the rotor naturally rotates about the vertical shaft in a predefined direction. The approaching flow could be from any spatial direction, and could have changing speed and direction in any fashion, but the unidirectional behavior of the rotor never changes. Such a behavior guarantees a unidirectional performance of the rotor in waves, where the water flow is omnidirectional and constantly evolving. In validating the proof of concept and characterizing the rotor's unidirectional performance, experiments were carried out under various flow conditions. Specifically, three types of flows were employed: horizontally oscillating flow, vertically oscillating flow, and orbital flow along a circular path in a vertical plane. The three flows were actually created by translating the rotor in still water, with the first two to characterize the rotor's responsiveness to the flow direction and the third one to simulate rotor interaction with deep waves. For each flow type, different rotor configurations/blade formations were examined under various testing parameters. For all the cases, the rotor shaft was kept vertically all the time. The experimental results are discussed in details in the paper.

Key words: wave energy converter, WEC, vertical axis, unidirectional rotor.

* Address all correspondence to this author. Email: yingchen.yang@utrgv.edu

1. INTRODUCTION

Ocean waves are a rich source of renewable energy with much higher power density than winds. Energy harvesting from ocean waves, however, is much more difficult than from winds due to the complex flow nature. Various WEC technologies have been proposed or are under serious development, with some demonstrated promising potential [1]. Due to the undulating nature of waves, it is intuitive to let the waves drive a WEC for reciprocating motion, e.g., up-and-down motion (heave), back-and-forth motion (pitch), etc. Not surprisingly, the overly dominant WEC designs explored in industry belong to this reciprocating type, including the best known PowerBuoy [2] and Pelamis (defunct since 2014) [3]. A reciprocating WEC uses the resonance principle to enhance its efficiency. The resonant behavior, however, makes the WEC very frequency-specific. This is in contrast to the broad frequency range of the ocean waves. Note, though, that some frequency-tuning mechanisms are usually applied to this type of WECs, but the tuning range is very limited.

Fundamental wave dynamics reveals that in deep waves water particles move along vertically oriented circular orbits with a horizontal drift [4]. In utilizing this flow feature, some unidirectional rotary WEC designs have been realized. Examples include a Savonius WEC [5] and a cycloidal WEC [6]. This unidirectional WEC type is in contrast to the reciprocating type. The rotational axis of a unidirectional WEC is preferably aligned horizontally along the wave crest to take the full advantage of the water's vertical orbital motion. This alignment preference, however, greatly complicates the WEC structure with a realignment mechanism to cope with the changing wave propagation direction.

It is noteworthy that unidirectional WECs circumvent the frequency-specific nature as possessed by reciprocating WECs.

On the other hand, some reciprocating WECs (e.g., the heave type) have no needs for realignment with respect to the wave propagation direction. If these two behaviors could be jointly realized in one WEC design, then the elimination of the frequency tuning and/or realignment mechanisms would allow a much simpler WEC structure. In fact, an existing technology—the WaveRotor [7]—has demonstrated a WEC of this type. It is a vertical-axis unidirectional WEC.

The hydrodynamic design of a vertical-axis unidirectional WEC is drastically different from that of a horizontal-axis unidirectional WEC. Using simple waves as an example, ideally the orbital motion of water particles in absence of WECs is two-dimensional; the third dimension is along a horizontal direction (i.e., along the wave crest). For a horizontal-axis WEC, the preferred orientation is to match the WEC's rotational axis with that third dimension. As a result, wave interaction with the horizontal-axis WEC is dominantly two-dimensional. For a vertical-axis WEC, however, the rotational axis is always orthogonal to that third dimension. Therefore, wave interaction with the vertical-axis WEC is strongly three-dimensional. And, with respect to the vertical-axis WEC, the wave-driven water motion even in absence of the WEC is truly omnidirectional and dynamically changing.

Commonly a unidirectional WEC, either with a horizontal axis or a vertical axis, has a rotor as its key component to interact with waves and perform unidirectional rotation for energy harvesting. With focus on the vertical-axis case, an associated rotor surely has its shaft vertically aligned. Then to utilize an omnidirectional water flow to drive it for unidirectional rotation, it is expected that the flow from any direction should always make the rotor rotate in one predefined direction along the shaft. Obviously, realizing such a rotor is challenging, and the hydrodynamic design of the rotor blades (i.e., blade shape and blade configuration) plays a critical role.

Using a unidirectional flow to drive a rotor for unidirectional rotation has long been used in a variety of engineering applications (e.g., a horizontal-axis wind turbine). For such a general rotor, if the flow direction reverses, the rotation direction of the rotor also reverses. In some special applications, however, it is expected that a bidirectional flow can drive a rotor for unidirectional rotation. The rotor of this type is called a Wells' rotor [8]. Now to enable a vertical-axis unidirectional WEC, it is further expected to have an omnidirectional flow to drive a rotor for unidirectional rotation. The WaveRotor has demonstrated the feasibility [7]. Most recently, the first author has been leading the effort in developing more rotors of this type [9, 10].

In the present work, a new vertical-axis unidirectional rotor design has been explored experimentally. Various rotor configurations and testing parameters were employed. The preliminary results were analyzed to gain fundamental understanding of the rotor's hydrodynamic performance.

2. EXPERIMENTAL SYSTEM

All experiments were carried out in still water in a wave flume of inner dimensions 15m (L) × 1m (W) × 1.3m (H). A special machine developed in house was employed to drive a rotor for three types of translation motion – vertical oscillation, horizontal oscillation, and orbital motion along a circle in a vertical plane. The vertical and horizontal oscillations were used to characterize the rotor's directional responsiveness. The orbital motion simulated wave-rotor interaction in deep waves with the horizontal drift neglected. In all the motion types, the rotor shaft was maintained in a vertical direction all the time. And, the rotor can freely rotate about the shaft with only friction from two supporting bearings.

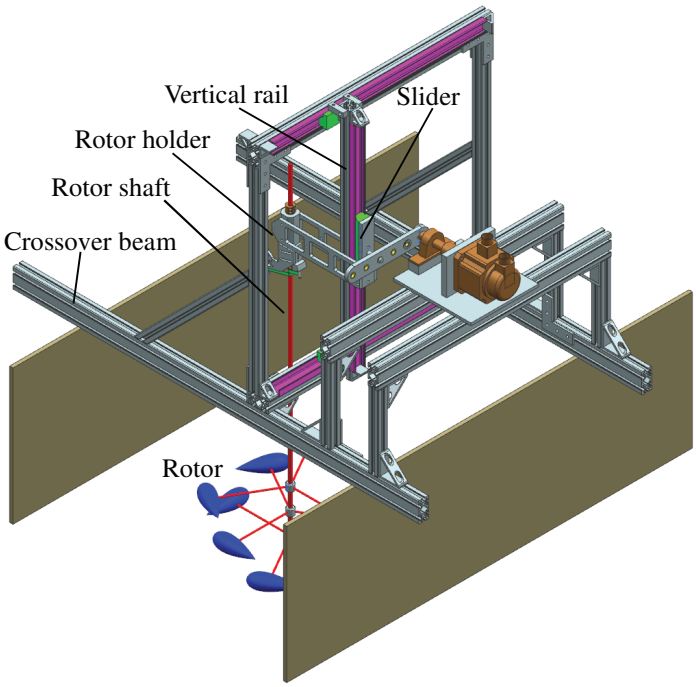

Figure 1: Experimental setup.

Fig. 1 shows the experimental setup for the circular motion case. In this case, the rotor holder is mounted to the slider. By mounting the rotor holder to the vertical rail instead of to the slider, the rotor would perform horizontal oscillation. Based on the setup for horizontal oscillation, by turning the machine by 90° along a cross beam (with an added supporting beam upon turning, not shown) and realigning the rotor shaft vertically (with the rotor holder still mounted to the same rail via a specially designed adaptor), the rotor's vertical oscillation is realized. For each of the three periodic motion types realized, the vertical moving range of the rotor simulates the wave height H (peak-to-pick) and the frequency represents the wave frequency f_W. Therefore, H is herein used to denote twice the amplitude for the oscillation (either horizontal or vertical) and the diameter for the circular motion, and f_W is used for the frequency of the rotor's periodic motion (horizontal, vertical, or circular).

To configure the vertical-axis rotor for unidirectional rotation in waves, nine identical blades were employed. An individual blade was formed by revolving a symmetrical hydrofoil NACA0035 along its chord line. The length (chord length) and the maximum diameter (D) of the blade were 152.4 mm and 53.3 mm, respectively. 3-D printing was used to make the blades. Upon completion, the nine blades were connected to a shaft through spokes and formed a nine-blade rotor. By rearranging blades in different ways, three rotor configurations have been realized, as illustrated in Fig. 2.

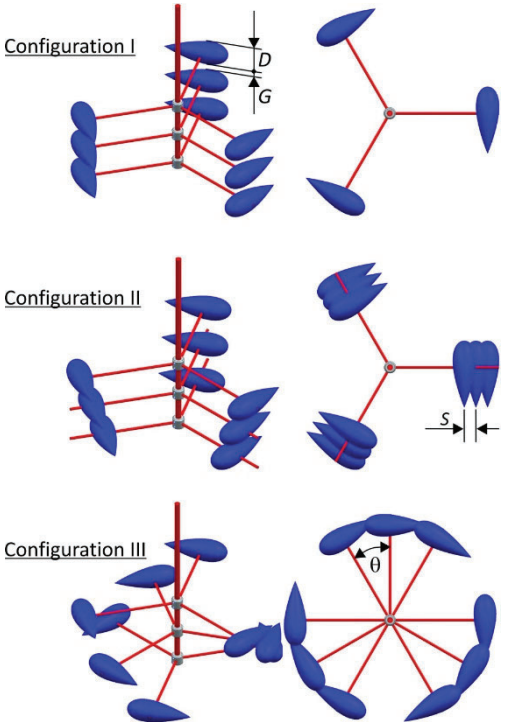

Figure 2: Perspective and top views of three rotor configurations.

The three rotor configurations in Fig. 2 had the same rotor diameter (the diameter of the maximum circular swept area when rotating), which was 500 mm. The diameter D of an individual blade is defined in Configuration I, $D = 53.3$ mm. A gap G is also defined in Configuration I. In testing Configuration I, the normalized gap G/D were varied in the range $0.25 \le G/D \le 2.0$. Configurations II and III were all tested at a fixed value of $G/D = 1.0$ only. Configuration II is a tapered variation of Configuration I by sliding blades inwards along the radial direction by a distance of $S = 0.5D$, as defined in Fig. 2. Configuration III is a spiral variation of Configuration I as shown in Fig. 2 with $\theta = 30°$.

With the current focus on validating proof of concept and gaining preliminary understanding, all the three rotor configurations were tested under a free-wheeling condition. Specifically, the energy extracted from waves was only used to overcome friction of bearings and drag from spokes and blades. In the next phase (not covered in this paper), a power takeoff simulator will be integrated with the rotor to further test the loading effect.

In characterizing the rotor's performance on unidirectional rotation, obtaining time traces of the rotor's angular velocity is of great importance. An iPhone 6 Plus was used for this purpose. It was mounted to the rotor holder in Fig. 1 (iPhone not shown). During the experiments the iPhone translated together with the rotor and, thus, was capable of videotaping the rotor's rotation only. A framing rate of 240 fps (slow motion for sharper images) were employed in videotaping. For each experimental run, a 75-second video was taken. The videos were then manually processed frame by frame at a sample rate of 30 samples per second to derive the angular velocity. Since the interested frequency components for most tested case were below 1 Hz (as to be discussed in the following), a low-pass filter with a cut-off frequency of 2.6 Hz was employed in data processing.

3. RESULTS AND DISCUSSION

For Configuration I of the rotor performing circular motion, the gap effect on the averaged angular velocity was examined first. Fig. 3 shows the variation of the averaged angular velocity $\overline{\omega}$ versus the normalized gap G/D at three values of f_W. In general, a larger gap between two adjacent blades along the shaft direction yields a higher angular velocity of the rotor. This is particularly true when $G/D < 1$. Obviously, interaction among the blades weakens, rather than strengthens, their individual contribution in driving the rotor for unidirectional rotation. With increasing G/D, such negative effect gradually reduces. Beyond, $G/D = 1.0$, the interaction effect becomes much less noticeable.

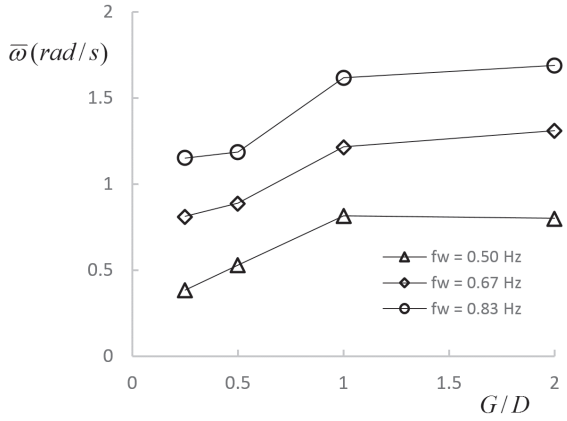

Figure 3: Gap effect on the averaged angular velocity for Configuration I in circular motion. $H/D = 6$.

The gap not only affects the averaged angular velocity of the rotor, but also alters the pattern of the instantaneous angular velocity ω. Fig. 4 compares four time traces of ω at four values of G/D. All the other experimental conditions are the same. The four time traces exhibit two common behaviors of the rotor – the absolute unidirectional rotation and the strong rotation fluctuation. Further examination on the amplitude spectra of the four time traces tell differences, as illustrated in Fig.5.

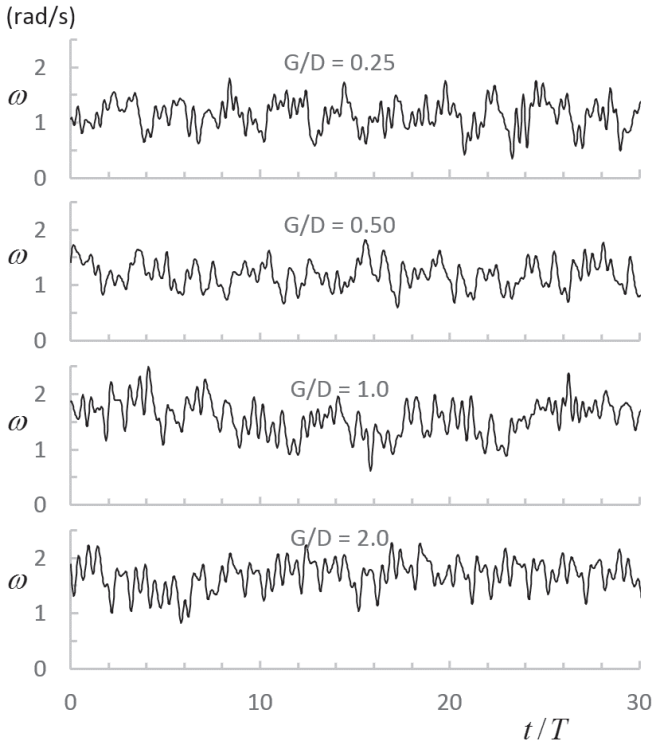

Figure 4: Typical time traces of ω within 30 periods ($T = 1/f_W$) for Configuration I in circular motion at four given values of *G/D*. Other parameters: $f_W = 0.83$ Hz, *H/D* = 6.

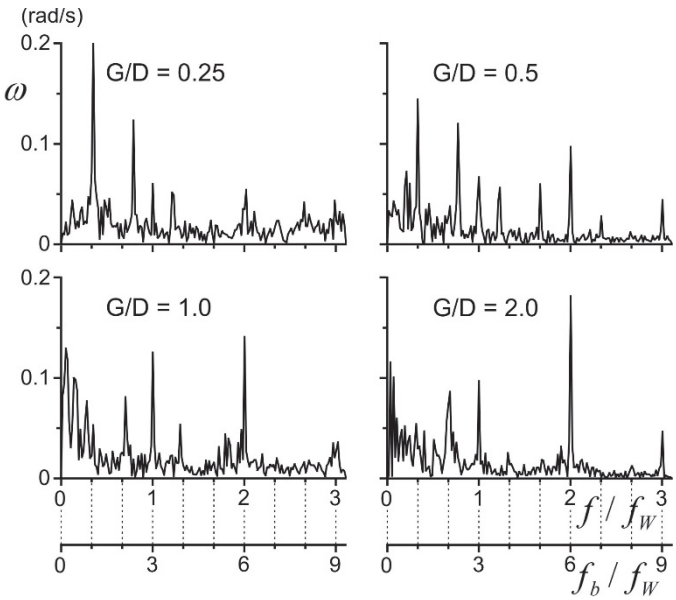

Figure 5: Amplitude spectra for the four time traces in Fig. 4.

Specifically, the two peaks at $f/f_W = 1$ and 2 in each spectrum are due to the periodic circular translation of the rotor in water. Very interestingly, at *G/D* = 0.25, the two peaks are very weak (still clearly detectable though). Then the larger *G/D* goes, the more dominant the two peaks become. On the other hand, at *G/D* = 0.25, two peaks at $f/f_W = 0.35$ and 0.79 are overall dominant. Note that the second one is not a harmonic of the first one. Then with increasing *G/D*, the two peaks gradually weakens until they lose the dominance. They also slowly shift to slightly lower frequencies when *G/D* increases. These two peaks are attributed to the strong interaction among individual blades. In addition to the normalized frequency f/f_W, Fig.5 also provides another frequency measure – f_b/f_W, where f_b is the blade pass frequency of the rotor configuration I.

Evidently, both the amplitude spectra of the instantaneous angular velocity (Fig. 5) and values of the averaged angular velocity (Fig. 3) suggest that, beyond *G/D* =1.0, the gap effect has been significantly reduced. For this reason, for all the rotor configurations to be further discussed in the following, the normalized gap is fixed at *G/D* = 1.0.

With the normalized gap fixed at *G/D* = 1.0, three rotor configurations are compared the next. Fig. 6 shows the variation of $\overline{\omega}$ versus f_W at three values of *H/D* for each rotor configuration. Regardless of rotor configurations and values of *H/D*, a nearly linear trend of $\overline{\omega}$ versus f_W is always observed. By comparing all the trend lines together, the normalized "wave height" *H/D* demonstrates a strong impact on $\overline{\omega}$; the trend lines are aggregated into three groups by the three values of *H/D*. The rotor configuration also plays an important role. At *H/D* = 2, the values of $\overline{\omega}$ are generally low, and there is not much of difference among the three configurations. At *H/D* = 4 and 6, however, the difference is evident. Specifically, with all other parameters fixed, Configuration I yields the strongest rotation, whereas Configuration II leads to the weakest rotation.

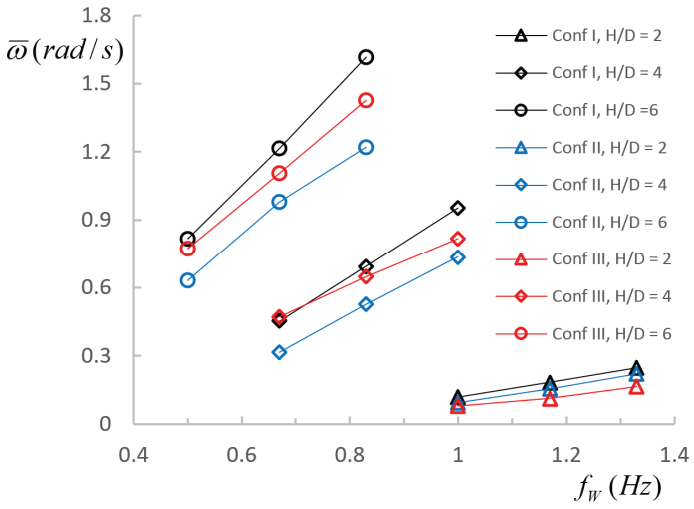

Figure 6: Comparison of $\overline{\omega}$ versus f_W for different rotor configurations in circular motion at different values of *H/D*.

More comparisons for the three rotor configurations are provided in Fig. 7 and Fig. 8 in terms of time traces and amplitude spectra. Following the order of Configurations I, II and III in Fig. 7, the time traces become more and more

organized with less and less fluctuation. Such an observation is consistent with the corresponding spectra in Fig. 8. Special attention should be paid to Configuration III; the spectrum has two small peaks at $f/f_W = 0.23$ and 0.74, a hardly detectable peak at $f/f_W = 1$, and an overly dominant peak at $f/f_W = 2$. The first two peaks are due to the interaction among the rotor blades, and the other two are directly associated with the wave motion. There are two major differences between this spectrum for Configuration III and the other two spectra for Configurations I and II: (i) blade interaction results in two clearly defined yet weak peaks for configuration III, but noisy and relatively strong spectra (particularly at the low end) for Configurations I and II; and (ii) the peak at $f/f_W = 1$ almost disappears for Configuration III but is very strong for Configurations I and II.

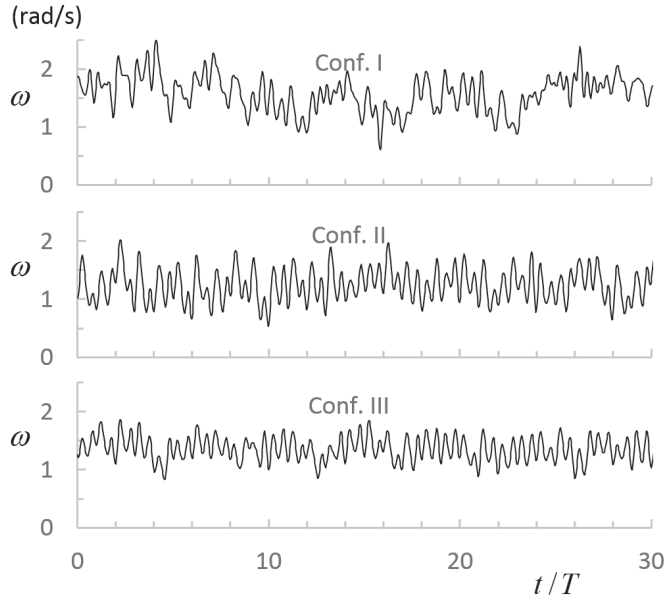

Figure 7: Comparison of time traces for three rotor configurations in circular motion at $f_W = 0.83$ Hz and $H/D = 6$.

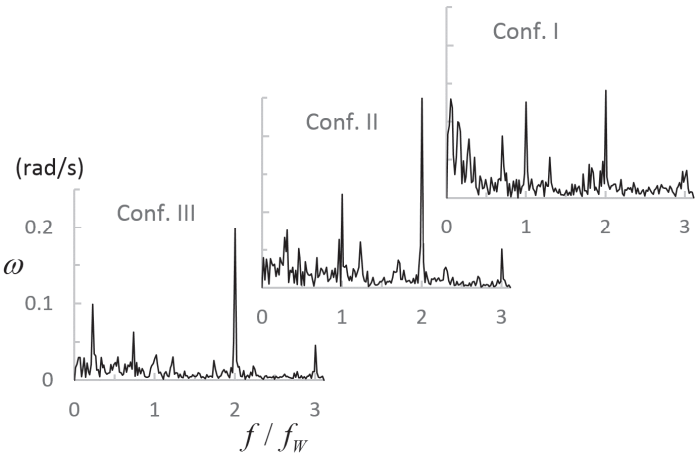

Figure 8: Amplitude spectra for the three time traces in Fig. 7.

After evaluating the fluctuation of the instantaneous angular velocity ω using the standard deviation (SD), the averaged angular velocity $\overline{\omega}$ and the standard deviation SD for the three time traces in Fig. 7 are presented in Fig. 9. Apparently, Configuration I has the fastest yet most fluctuating rotation, and Configuration III has a moderate but smoothest rotation.

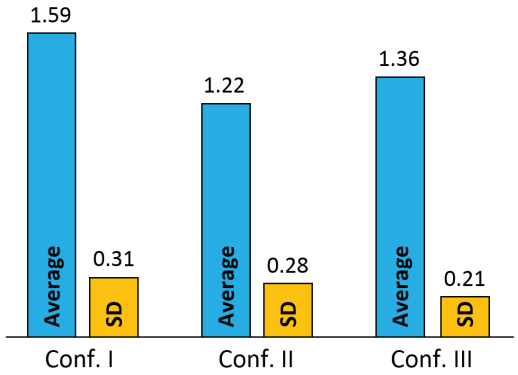

Figure 9: Average and standard deviation (SD) for the three time traces of ω in Fig. 7. Units in rad/s.

To realize unidirectional rotation of a vertical-axis rotor in omnidirectional flows, and to guide the hydrodynamic optimization of the rotor, it is important to understand how component flows contribute to the unidirectional rotation. For these purposes, the three rotor configurations were also tested under vertical and horizontal oscillations at the same simulated wave heights as for the circular motion. A comparison of the averaged angular velocities was presented in Fig. 10. In general, the rotor responded to the vertical oscillation and horizontal oscillation drastically differently. Simply, all the three configurations responded to the horizontal oscillation very poorly, but they all responded to the vertical oscillation surprisingly well. For Configuration I, the vertical oscillation resulted in an $\overline{\omega}$ that was lower than but close to the $\overline{\omega}$ obtained

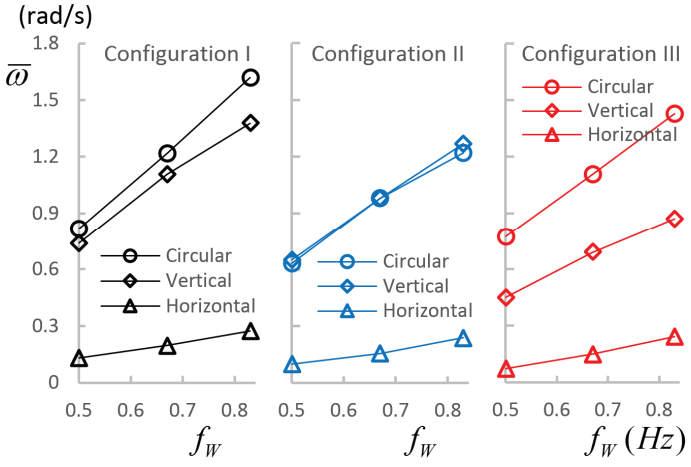

Figure 10: Comparison of rotor responsiveness to component flows among the three rotor configurations in terms of $\overline{\omega}$ versus f_W.

in the circular motion. For Configuration II, the vertical oscillation was just as good as the circular motion. For Configuration III, however, the vertical oscillation did far worse than the circular motion.

The time traces of ω and their spectra in vertical and horizontal oscillations reveal deeper understanding, as reflected in Figs. 11 through 14. Fig. 11 compares the time traces of ω for the three configurations in the vertical oscillation. All the three traces indicate unidirectional rotation with no reversal, and they all are close to a sinusoidal waveform. The corresponding spectra are very clean with two sharply defined dominant peaks at f/f_W = 1 and 2, as shown in Fig. 12. Such simple and strong rotor responses to the vertical oscillation are in comparison to the complex yet robust responses to the circular motion (Figs. 7 and 8). It is noteworthy though, that the rotation fluctuation in the vertical oscillation is much stronger than in the circular motion.

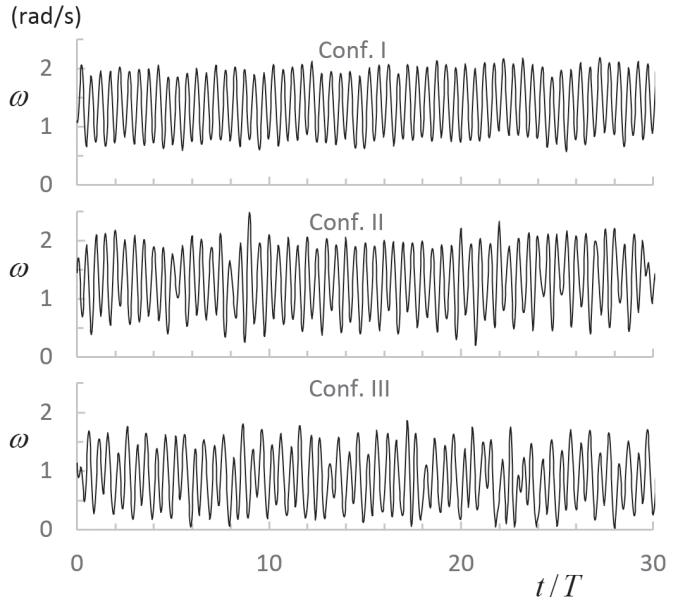

Figure 11: Comparison of time traces for three rotor configurations in vertical oscillation at f_W = 0.83 Hz and H/D = 6.

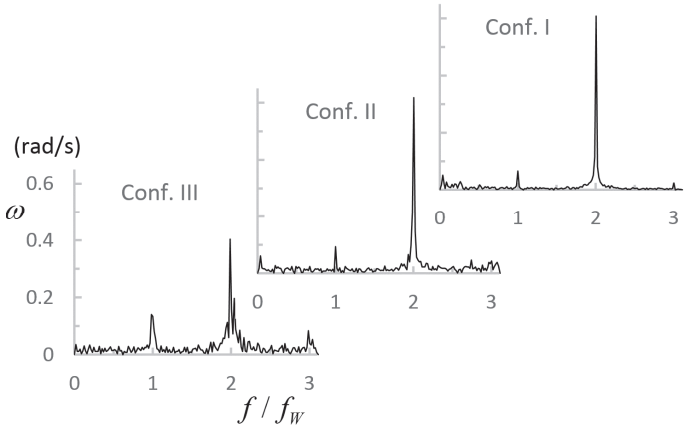

Figure 12: Amplitude spectra for the three time traces in Fig. 11.

Behaving quite differently from the case of vertical oscillation, the three rotor configurations lost their capability to perform unidirectional rotation in horizontal oscillation. As indicated by the time traces in Fig. 13, strong rotation reversal occurred very frequently for Configurations I and II, but only mild rotation reversal was observed for Configuration III and it happened less frequently than the other two. In any case, rotation reversal is unwanted in developing a unidirectional rotor. Even though the reversal did not occur in the circular motion (which simulates the wave motion), its occurrence in the horizontal oscillation suggests that improvement is needed in the present rotor designs (Configurations I, II, and III) for a better horizontal responsiveness.

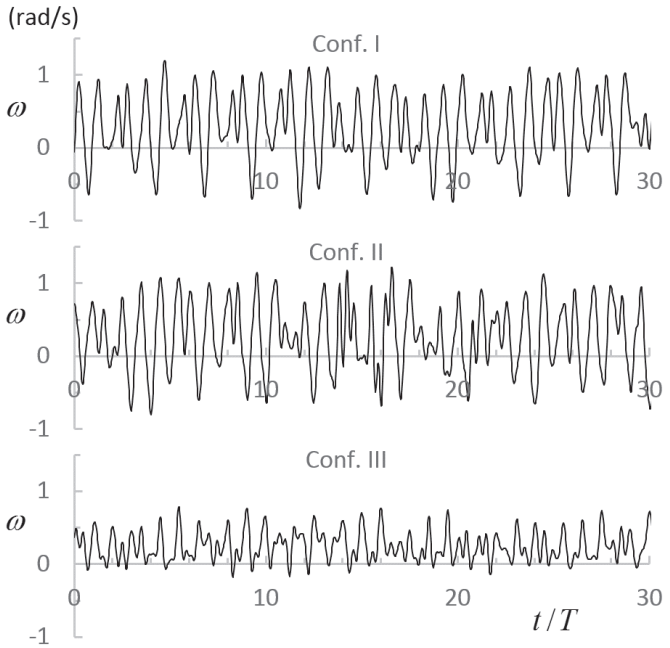

Figure 13: Comparison of time traces for three rotor configurations in horizontal oscillation at f_W = 0.83 Hz and H/D = 6.

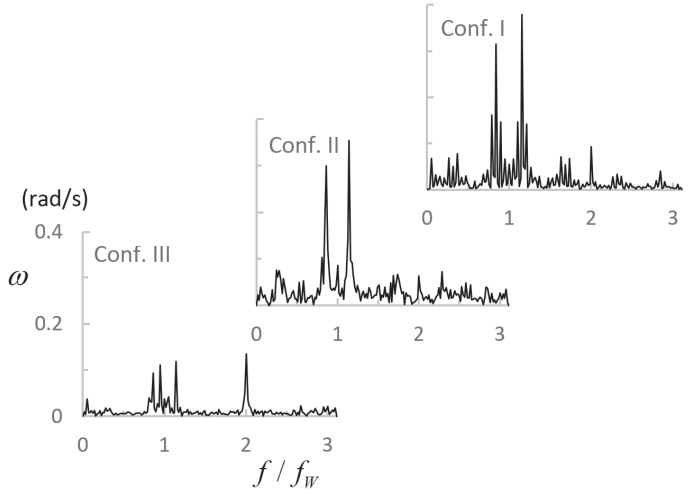

Figure 14: Amplitude spectra for the three time traces in Fig. 13.

Fig. 14 presents the amplitude spectra for the three time traces in Fig. 13. The spectra for Configurations I and II show two dominant peaks at $f/f_W = 0.85$ and 1.15; peaks at $f/f_W = 1$ and 2 are trivial, if ever noticeable. In contrast, for Configuration III all the four peaks at $f/f_W = 0.85$, 1.15, 1, and 2 are nearly equally dominant.

4. CONCLUSIONS

In an attempt to use omnidirectional flows to drive a rotor for unidirectional rotation, a new vertical-axis rotor has been explored for energy harvesting from ocean waves. The rotor consists of nine identical blades, with each shaped by revolving a symmetrical hydrofoil about the chord line. Three rotor configurations were realized by arranging the nine blades in different layouts. Experiments were conducted by translating the three rotor configurations in still water in three motion types – the circular motion in a vertical plane, the vertical oscillation, and the horizontal oscillation. Experimental results show that all the three rotor configurations are capable of performing unidirectional rotation about the vertical axis in both circular motion and vertical oscillation. The difference is reflected on the rotor's rotation speed and rotation steadiness. Nonetheless, rotation reversal was observed for all the three rotor configurations in the horizontal oscillation. An improved rotor design is needed to eliminate such rotation reversal for a stronger unidirectional rotation in omnidirectional flows.

REFERENCES

[1] Falcao, A., "Wave energy utilization: A review of the technologies," *Renewable and Sustainable Energy Review*, 14, 899-918, 2010.

[2] Mekhiche, M.and Edwards, K., "Ocean power technologies PowerBuoy: system-level design, development and validation methodology," in *Proceedings of 2nd Marine energy Technology symposium*, Seattle, WA, April 15-18, 2014.

[3] Pizer, D., Retzler, C., Henderson, R, Cowieson, F., Shaw, M., Dickens, B., and Hart, R., 2005. "Pelamis WEC – recent advances in the numerical and experimental modelling programme," in *Proceedings of the 6th European Wave and Tidal Energy Conference*, 373-378, 2005.

[4] Pickard, G. L. and Pond, S., *Introductory Dynamical Oceanography*, 2nd ed, Oxford: Elsevier Butterworth-Heinemann, 1983.

[5] Ahmed, M. R., Faizal M. and Lee, Y. H., "Optimization of blade curvature and inter-rotor spacing of Savonius rotors for maximum wave energy extraction," *Ocean Engineering*, 65, 32-38, 2013.

[6] Siegel, S. G., Fagley, C., and Nowlin, S., "Experimental wave termination in a 2D wave tunnel using a cycloidal wave energy converter," *Applied Ocean Research*, 38, 92-99, 2012.

[7] Rossen, E. A., Scheijgrond, P. C. and Mikkelsen, R., "Development and model test of a combined Wells-Darrieus wave rotor," in *Proceedings of 4th European wave Energy Conference*, Aalborg University, Denmark, 2000.

[8] Raghunathan, S., "The Wells air turbine for wave energy conversion," *Progress in Aerospace Sciences*, 31, 335-386, 1995.

[9] Yang, Y., Diaz, I., Morales, M., and Obregon, P., "A vertical axis wave turbine with cup blades," in *Proceedings of ASME 34th International Conference on Ocean, Offshore and Arctic Engineering,* St. John's, NL, Canada, May 31 – June 5, 2015.

[10] Yang, Y., Diaz, I., and Soto, S., "A vertical axis wave turbine with hydrofoil blades," in *Proceedings of ASME 2016 International Mechanical Engineering Congress & Exposition,* Phoenix, AZ, November 11-17, 2016.